OPTIMIZATION OF A COMPTON SCATTERER FOR HARD X-RAY WEAPONS EFFECTS SIMULATION IN AN ICF FACILITY

THESIS

Russell L. Tinsley
Captain, USAF
AFIT/GNE/ENP/90M-7

DEPARTMENT OF THE AIR FORCE
AIR UNIVERSITY
AIR FORCE INSTITUTE OF TECHNOLOGY

Wright-Patterson Air Force Base, Ohio

AFIT/GNE/ENP/90M-7

OPTIMIZATION OF A COMPTON SCATTERER FOR HARD X-RAY WEAPONS EFFECTS SIMULATION IN AN ICF FACILITY

THESIS

Russell L. Tinsley
Captain, USAF
AFIT/GNE/ENP/90M-7

AFIT/GNE/ENP/90M-7

OPTIMIZATION OF A COMPTON SCATTERER FOR HARD X-RAY WEAPONS EFFECTS SIMULATION IN AN ICF FACILITY

THESIS

Presented to the Faculty of the School of Engineering

of the Air Force Institute of Technology

Air University

In Partial Fulfillment of the

Requirements for the Degree of

Master of Science

Russell L. Tinsley, B.S.

Captain, USAF

March, 1990

Approved for public release; distribution unlimited

AFIT/GNE/ENP/90M

Acknowledgements

In performing this project I had a great deal of help from others. I would like to thank Major Denis Beller, both for his help and his patience through the numerous delays. I also wish to thank Mike Tobin whose insight provided the path I followed. A very special thanks to Mike Sabochick who saw something in me that others did not see. His help was both tireless and indispensable. Finally, I wish to thank my parents for their prayers which saw me through all obstacles.

Russell L. Tinsley

Abstract

This ~~work~~ examined the optimization of a Compton scatterer for use in simulating hard X-ray effects in the proposed Laboratory Microfusion Facility (LMF). The LMF will produce inertial confinement fusion of deuterium-tritium pellets. The Compton scatterer is designed to reflect the X rays produced from the fusion toward a target. The scatterer should produce the maximum X-ray dose at the target while minimizing the neutron dose and gamma production. The scatterer must also control the dose rate by spreading the X-ray pulse to achieve a full width at half maximum on the order of 10s of ns.

The "current" geometry includes a spherical Compton scatterer made of lithium hydride enriched to 95.6% Lithium 6. This work explored various parabolic scatterers using Monte Carlo transport calculations performed on the MCNP program from Los Alamos National Lab. The parabolic shape was optimized to increase the X-ray dose at a silicone target by a factor of 7. The geometry also decreased the neutron and gamma doses to less than 1% of the X-ray dose while achieving an 80% uniformity of dose across a 1-meter-radius silicon disk.

No geometry has been found which meets the temporal specifications. By reducing the scatterer's density to one quarter nominal density, the dose distribution achieved a FWHM of 4.06 ns. All characteristics were improved in comparison to the spherical geometry but much work remains in spreading the pulse shape.

Table of Contents

List of Figures

List of Tables

OPTIMIZATION OF A COMPTON SCATTERER FOR HARD X-RAY WEAPONS EFFECTS SIMULATION IN AN ICF FACILITY

I Introduction

Background

ICF. Unlike nuclear fission reactions, fusion reactions occur at temperatures in the range of 40 million K. Confining fuel at this temperature is the primary concern in making fusion a feasible energy source. Approximately two-thirds of the fusion energy research currently conducted in the United States is based on the magnetic confinement approach i.e. the fuel is contained by magnetic fields during fusion. Inertial Confinement Fusion (ICF) is an alternative approach first conceived in the 1960's. The concept behind ICF is to compress fuel pellets to densities high enough that the fuel's own inertia would be sufficient to contain it (1:548).

ICF uses fuel pellets a few millimeters in diameter. A tremendous amount of energy is deposited symmetrically on the pellet in a very short time (1-10 megajoules in about 10 ns). The ablation of the outer edge of the pellet compresses the fuel to densities of about 1kg/cm^3. Converging

shock waves ignite the fuel at the center of the pellet, and produce an expanding burn wave that heats the rest of the fuel to ignition temperature (2:441).

The Laboratory Microfusion Facility (LMF) is a facility proposed by the Lawrence Livermore National Laboratory (LLNL) for research in ICF. The LMF could potentially provide ICF energy pulses on the order of 1 gigajoule (3:5). One possible application for this facility is in weapons effects testing, more specifically, X-ray simulation.

Space X-Ray Effects. The X-rays produced by ICF could be used to test weapons systems and components against the type of hard X-ray (>10 keV) pulses that a nuclear burst might deliver on a satellite or other space based system. Unlike energy production applications, X-ray simulation does not require a high energy gain to be economically feasible. In addition to providing test capabilities not currently available, the LMF would deliver these tests much more economically than underground testing and with higher frequency. In the face of a possible underground test ban, LMF is a promising option for the future of X-ray simulation.

The X-ray simulation is significant because of the degradation of electronic circuits through exposure to X-rays. The energy deposited in integrated circuits ionizes the silicon producing additional electron/hole pairs. The pro-

duction of mobile charge carriers at an NP junction can produce a transient current. If enough radiation energy is deposited, the induced current can exceed the signal current. The total energy absorbed (dose) determines the number of electron/hole pairs produced. The average energy deposited per electron hole pair produced is 3.6 eV for silicon.

$$\frac{(0.01\,J/kg/Rad(Si))(2.33g/cm^3)}{(3.6eV/pair)(1.6\times10^{-19}J/eV)} = 4.04\times10^{13}\frac{pairs}{cm^3Rad(Si)}$$

The photocurrents produced by the additional charge carriers is proportional to the carrier generation rate and is therefore proportional to the dose rate. Thus, both dose and dose rate are important to X-ray effects. (4:266-71)

Problem and Scope

To function as an X-ray simulator, the LMF must be capable of producing both a sufficient amount of energy fluence and the appropriate pulse shape. The ICF output pulse is essentially a delta function in time. In order to shape the pulse to its desired form a Compton scatterer is placed around the source so that the X-rays arrive at the target via different path lengths; this spreads the fluence to provide the desired dose rates.

The scatterer is made of lithium hydride because it has the highest number density of any solid. Because LiH is a low Z (atomic number) material, X-rays will not be attenuated as quickly as with a high Z material. Because hydrogen has approximately the same mass as the neutrons, it will help thermalize the neutrons and will not allow them to backscatter. By enriching the scatterer with ^{6}Li, the thermalized neutrons are absorbed by the following reaction

$$^{6}_{3}Li \quad (n,\alpha) \quad ^{3}_{1}T$$

This reaction is desirable because it does not produce gamma rays. (5)

The ICF group at LLNL has asked AFIT to look at various geometric shapes as potential designs for the Compton scatterer. Specifically, LLNL has asked for a shape which provides the largest X-ray dose in rads (Si) while neutron and gamma doses and dose rates are kept below 1% of the corresponding X-ray doses. The dose will be calculated on a silicon disk of 20 micron thickness and 1 meter radius. The desired X-ray dose rate distribution has a full width at half maximum (FWHM) on the order of 10s of ns. The FWHM and rise times are related to a path length difference by multiplying the times with the speed of light, 30 cm/nS. (6)

The fuel pellets to be used are Deuterium-Tritium pellets. The DT reaction produces an alpha particle, a neutron, and 17.6 MeV of additional energy (7:21). Exact details of the energy spectrum released after fusion are classified so unclassified spectrum are substituted. The energy output is assumed to be partitioned in an 8 to 1 neutron energy to X-ray energy ratio. The X-rays are assumed to be described by a 10 keV planckian distribution and the neutrons are represented by a simple histogram with the average neutron energy in the range of the 14.1 MeV characteristic of DT fusion.

The calculations are preformed using MCNP, a Monte Carlo neutron and photon transport code supplied by the Radiation Shielding Information Center (RSIC). LLNL has asked that the answers are calculated to within 1% standard deviation. (6)

Approach

There are an infinite number of possible geometries available, and there is no simple way to accurately predict the results other than with a full MCNP run. The runs are relatively slow and as such are not conducive to an iteration process where parameters are adjusted between runs, eventually converging on an optimum geometry.

Given a very limited time to examine different geometries the optimization was reduced to a handful of parameters which were varied individually to establish approximate optima. A definition of the "current" geometry is needed before a discussion of these parameters.

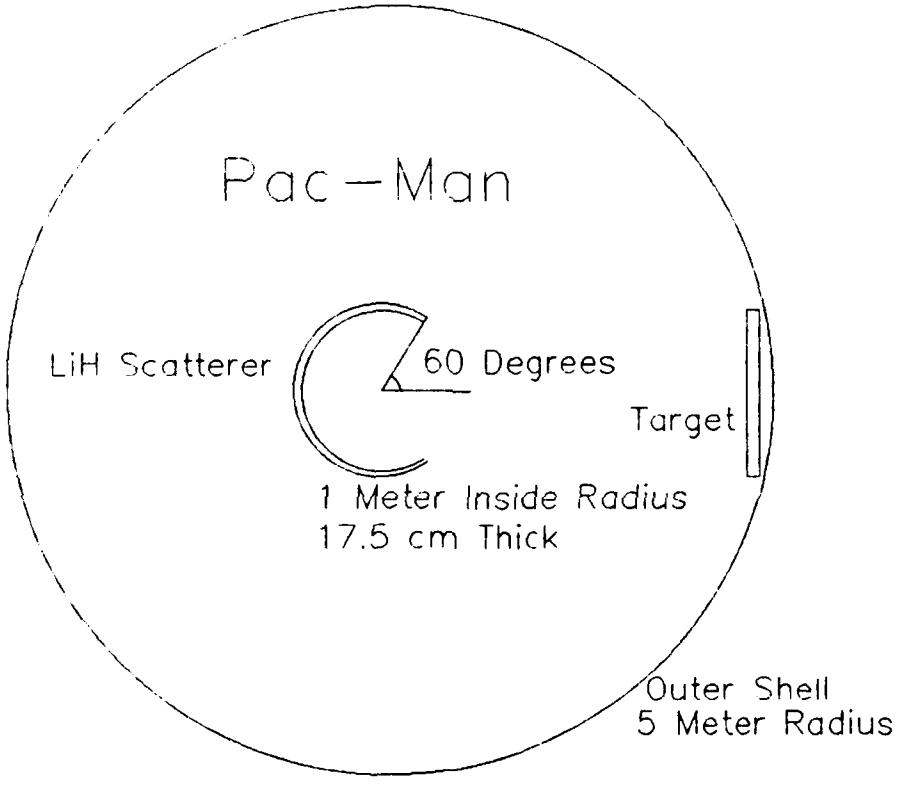

Figure 1.1: Pac-Man Geometry

The current geometry is the so called "pac-man" configuration. It consists of a spherical Compton scatterer, a neutron reflector and the outer walls. The Compton scatterer is composed of lithium hydride as mentioned earlier. The lithium is enriched to 95.6% ^{6}Li. The scatterer

has an inner radius of 1 meter and is 17.5 cm thick. The scatterer has a one-quarter solid angle opening in the direction of the target. A LiH cone (not shown in figure) is used to shield the target from direct neutron flux. This reflector exactly subtends the same angle as the target and has a length of one meter starting 25 cm from the center of the sphere. The outer wall is comprised of four layers at a five meter radius. The first layer is a 4-cm-thick hydrocarbon consisting of 38% hydrogen 23.5% carbon, 24.5% oxygen and 12.2% silicon. (Atomic percentages) The second and third tiers are 1 cm thick layers of lead and lithium respectively. The third layer is 50 cm of borated water, 65% hydrogen, 33.4% oxygen, 0.3% nitrogen and 1.3% boron. The target is a 20-micron-thick disk of silicon with one meterradius. (6)

LLNL suggested that a parabaloid geometry may provide a more efficient scatterer. With the exception of some runs conducted on the current geometry, all configurations used were paraboloids of some type. The first parameter considered was not specification of the parabaloid but the size of a tungsten tunnel to be added.

The addition of a tungsten tunnel will help protect the target from late time gamma rays created at the surface of the LMF by high energy neutrons. The tunnel must be designed to avoid obstructing the X-rays scattering off the

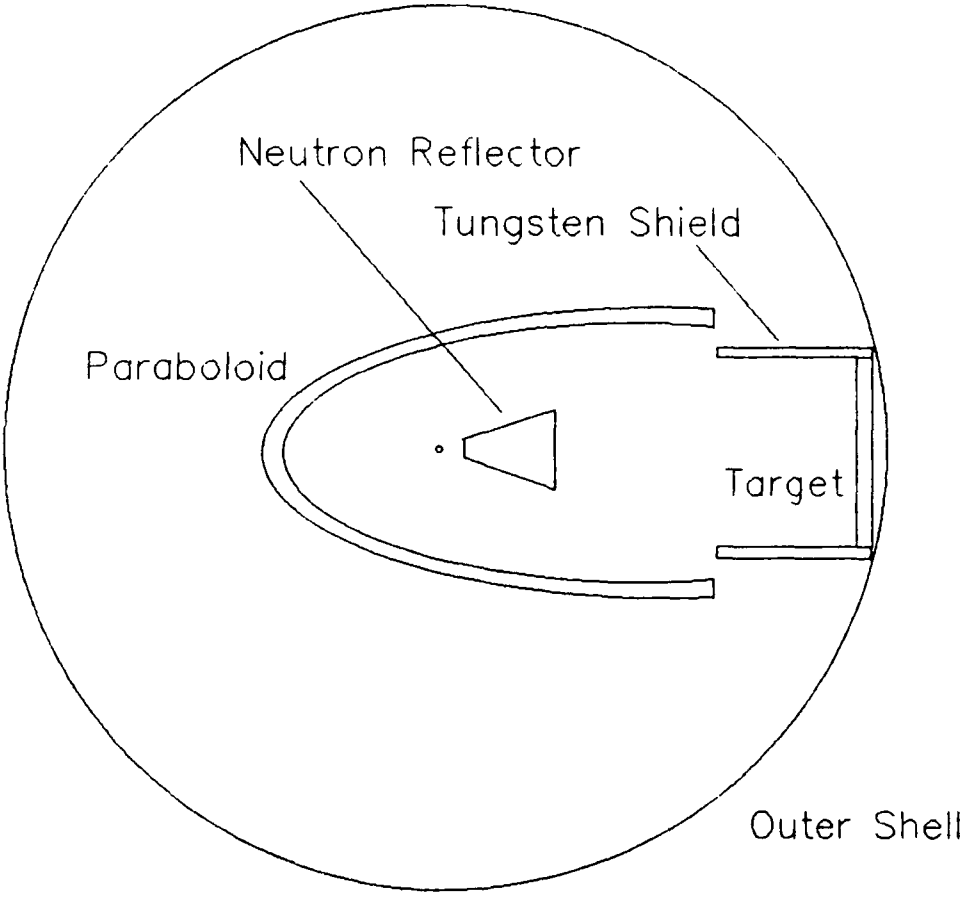

Figure 1.2: Paraboloid Geometry

LiH while partially shielding the target from the gammas approaching the silicon from larger angles. Tungsten is chosen for its ability to attenuate gamma rays and because it will not produce any additional neutrons or gamma rays. (6) The shield will be cylindrical with a 4 cm thickness. The length of this tunnel will be determined by testing various tunnel lengths for both neutron and photon doses. A standard paraboloid will be selected for this test. While there is no reason to assume that the optimum tunnel length

for one paraboloid will still be optimum when the scatterer configuration is altered, it is too computationally expensive to perform the calculations over for each geometry. Therefore the tunnel length chosen will remain static for all remaining tests.

After determining an appropriate tunnel length, the shape of the paraboloid will be tested. All the paraboloids are described by the equation

$$x = A(y^2 + z^2) - B \tag{1}$$

Where A and B are the parameters to be varied.

The final parameter to be examined will be the density of the scatterer. By changing the paraboloids density, the mean free path for the X-rays is proportionally adjusted. This will directly alter the path length travelled by the photons and should be an effective technique for calibrating the temporal characteristics of the pulse.

This approach is clearly inadequate for determining a final configuration to meet the required properties. It should however provide some insights into the effects of each of the parameters. The results may be an assistance in future efforts to optimize the geometry.

II MCNP

Basic Code

MCNP is a Monte Carlo transport code for neutrons and photons. It was written at Los Alamos National Laboratory and is distributed by RSIC. RSIC supplies the source code written in FORTRAN 77 and a set of hardware independent (type I) cross section libraries. The code comes ready to use for IBM Cray or Vax systems. The code includes a pre-processor which customizes the MCNP source code based on which machine is selected. With some effort the pre-processor can be modified to support other machines/operating systems. The type I cross section libraries can also be processed into system specific (type II) files. The type I files can be used with any hardware but the processed type II files allow entries to be read more quickly through direct access versus the sequential access method used in type I files.

MCNP allows three different modes of problems. Mode P is the photon transport mode. The neutron transport mode is mode N. Mode N P uses a neutron source but adds photon creation through n-gamma reactions. The mode along with the geometry, source, etc. are all defined in an input file called INP.

The geometry is described by defining cells and surfaces. The surfaces are defined by first and second degree polynomials in x, y, and z where a point is on the surface if it satisfies the equation $F(x,y,z)=0$. A point is said to have a positive or negative sense with respect to the surface if $F(x,y,z)>0$ or $F(x,y,z)<0$ respectively. The cells are defined by the positive and negative senses of these surfaces and with logical operators such as unions, intersections, and exclusion.

The use of inner and outer surfaces makes the parabolic geometry difficult to represent. A constant thickness cannot be represented by a second paraboloid surface. Instead an approximate shape is used which maintains a rough estimate of the desired thickness. The outer surfaces used are shown in appendix A.

Monte Carlo Techniques

Monte Carlo codes are used to simulate statistical processes that are too complex to be modeled deterministically. The results are determined by following particles from birth to death by statistical sampling of probability distribution functions. The MCNP manual defines the five "rules" of performing a Monte Carlo calculation as:

> Sample the source well
>
> Lost information cannot be recovered
>
> Question results for stability and reliability
>
> Be conservative and cautious with biasing
>
> The number of histories is not indicative of the quality of the answer(8:1)

Rule one recommends the use of an adequate number of particle histories to ensure that the sample particles match the distribution function the source is describing. The second rule is a reminder to specify all output options that are needed to interpret the results. The fourth rule suggest that variance reduction techniques be used judiciously.

The third and fifth rules point to the utility of the fractional error R which is calculated for every tally MCNP makes.

$$R = S_{\bar{x}} / \bar{x}$$

R represents the normalized uncertainty of a tally and provides a sense of confidence in the value of the tally. If a calculation is well behaved the fractional error will decrease proportional to $1/(N)^{\frac{1}{2}}$ where N is the number of particle histories. R is calculated from the second moment about the mean and for a sufficiently large number of histories, the central limit theorem states there is a probability of .6 that:

$$\bar{x}(1 - R) \leq \mu \leq \bar{x}(1 + R)$$

where μ is the true mean of the tally. This error estimate represents only the uncertainty in the calculation caused by sampling the true distributions with a finite number of particles. Any inaccuracies in modeling the true physical processes are not reflected in R. The number R is itself only an approximation of the relative error. A large value of R indicates an uncertainty in its estimation as well. The MCNP manual offers rules for interpreting R; they are listed in table 2.1.

Table 2.1: Interpreting Relative Error in MCNP

Range of R	Quality of the Tally
0.5 to 1	Not meaningful
0.2 to 0.5	Factor of a few
0.1 to 0.2	Questionable
<0.1	Generally reliable

Related to the relative error is another useful number, the figure of merit (FOM). The FOM is defined by the equation

$$FOM = 1/(R^2 T)$$

where T is the CPU time used. This value quantizes the efficiency of a calculation. The figure of merit should remain approximately constant for any number of particle histories. If it is not, the value of the tally is not to be trusted. (8:6-8)

Variance Reduction

MCNP offers numerous variance reduction techniques designed to raise the FOM by decreasing the CPU time needed to achieve a given value of R. The basic theory behind

these practices is to spend more time following "important" particles and less time following "unimportant" particles. Here, important/unimportant may refer to the level of contribution a particle will make to a tally or to the adequacy of the sampling of a certain parameter. Among the techniques used were Russian roulette, splitting, cutoff, and point/ring detectors.

Russian roulette is applied to relatively unimportant particles. A particle experiencing Russian roulette has a certain probability of being killed but, if it survives its weight is increased by a factor corresponding to the kill probability. Thus the total particle weight is preserved but less computer time is spent because of the reduction of particles. Russian roulette can be applied to particles that enter relatively unimportant cells, particles whose weight is too low to make a significant contribution, particles in an unimportant energy bin, etc.

Splitting is the antithesis of Russian roulette. It involves splitting a particle into multiple particles of less weight in order to better sample a certain energy range or cell.

Cutoff saves CPU time by terminating particles if their energy falls below a certain minimum or if it survives for a length of time such that it is no longer of interest.

By specifying a point or ring detector, MCNP will calculate a contribution every time a particle scatters based on the probability of scattering toward the detector and the attenuation factors. Point detectors can calculate flux without actually having any particles reach the detector. For problems with axial symmetry, such as this, MCNP recommends the use of ring detectors. The ring detector is a circle of specified radius. A point on the circle is selected randomly for each contribution calculation. (8:8-12)

Cross Sections

The basic set of cross section files consists of BMCCS, D91, ENDL85, MCPLIB and TMCCS1. BMCCS is apparently an acronym for basic Monte Carlo cross sections, D91 contains discrete energy cross sections, ENDL85 is the 1985 version of the Evaluated Nuclear Data Library compiled at LLNL. MCPLIB is used for photon cross sections, and TMCCS provides cross sections for thermal neutron interaction with molecules and crystalline solids. (8:526-31) With the exception of the D91 tables, all of these libraries are continuous-energy libraries that can be interpolated with less than 1% error.

The MCPLIB is the most simple because photons interact on an atomic scale, reactions depend only on the atomic number of the material since the reactions actually occur with the electrons surrounding the nucleus. The neutron tables are more complex since different isotopes of the same element may have different reactions with neutrons. The N P mode requires neutron tables that include photon production information. The MCNP manual recommends careful consideration be given to the cross section library used in neutron transport problems but it provides little assistance in making that selection. MCNP will choose a default library if none is specified, but the default is simply the first table it locates. A different table can be specified for each material used in a problem. (9:15-21)

The cross sections were the source of one bug not yet repaired in the code. Only the BMCCS tables worked properly for hydrogen in gamma-production problems. When other tables were specified, arithmetic exceptions occurred during the calculations of scattering angles.

Input Defaults

The three main elements of an MCNP input file are the geometry, the source specification, and the tally specifications.

The basic geometry usually remained static except for the scatterer shapes used. One exception was the neutron shield. During runs where tunnel lengths were varied, the angle of the shield was adjusted to allow no unscattered flux into the mouth of the tunnel.

The photon input spectrum was an approximation of a 10-keV Planckian. MCNP requires the source to specified in terms of the relative probability a particle will be in a certain energy bin. The number of photons in a given bin is determined by the equation

$$\int_{E}^{E+\Delta E} \frac{E^2 dE}{e^{h\nu/KT} - 1}$$

The equation was integrated numerically on a spreadsheet using the forward rectangular rule. The inputs do not have to be normalized for MCNP. The results are shown in figure 2.1.

The neutron energy distribution was specified as a histogram on early runs. Later runs invoked one of MCNP's built in source distribution functions, the Gaussian-fusion energy spectrum. This spectrum is described by the equation

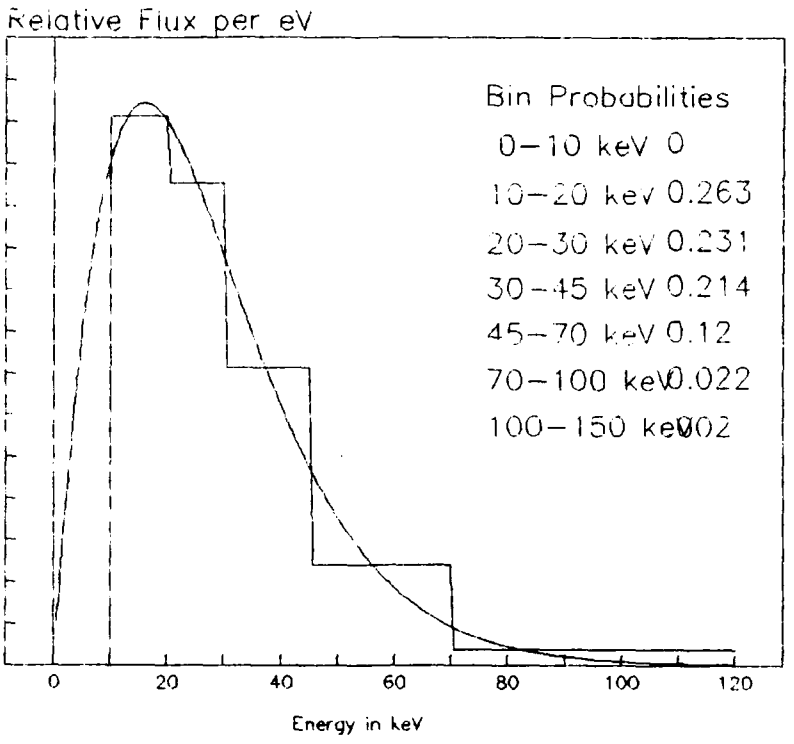

Figure 2.1: 10-keV Planckian Spectrum

$$p(E) = Ce^{-((E-b)/a)^2}$$

where a and b are the width and average energy in MeV. The width a was set to 0.5 MeV. By specifying a b value of -1 MCNP defaults to the average energy for DT fusion at 10 keV.

The output of an MCNP calculation is presented in terms of the tallies specified in the input file. MCNP allows five different tally types as displayed in table 2.2.

Type F5 provides the most accuracy as discussed previously. Unfortunately F5 tallies can not be used to calculate a dose

Table 2.2: Tally Types

Type	Description	Units
F1	Current integrated over a surface	particles or MeV
F2	Flux averaged over a surface	particles/cm^2 or MeV/cm^2
F4	Flux at a point or ring detector	particles/cm^2 or MeV/cm^2
F5	Flux averaged over a cell	particles/cm^2 or MeV/cm^2
F6	Energy deposition averaged over a cell	MeV/g (8:221)

or dose rate. In order to reduce the relative error to a few percent, a ring detector needs 50,000 particle histories. MCNP takes approximately 40 minutes of CPU time to run a 50,000 particle ring detector calculation for these geometries. A dose calculation requires even more particles to achieve similar accuracy because particles must actually enter the cell to contribute to the tally. To conserve time, all runs were preformed as F5 tally types in MeV/cm^2. The pulse shapes of the Energy flux should be virtually identical to the dose rate results. Similarly, the total energy fluence incident at the detector should be approximately proportional to the dose since the sources are identical. Dose/dose rate calculations will be performed only once, on the final geometry.

Neutron and gamma calculations are performed in the same manner. Unfortunately, the ratio of dose to energy incident will be different for all three particles: neutrons, gammas and x rays. It will be impossible to estimate the neutron to X ray or gamma to X-ray dose ratios from the F5 tallies. No comparison needs to be made for dose rate ratios. Since the neutrons are relatively slow particles compared with x-rays moving at the speed of light, the neutron dose will be spread over a longer time. This means the neutron and gamma dose rates are assured of being less than 1% of the X-ray dose rates provided the goal of a 1% dose ratio is met.

The X-ray runs partition the dose into time bins at 1 nS intervals. Since only a fraction of the particles contribute to any one time bin, the relative errors within the time bins are higher than for the total dose. The relative errors could be reduced by widening the bins but other information is lost. By widening the time bins, the pulse shape is described by fewer points and thus is not well resolved. The only solution is to raise the number of particle histories (assuming variance reduction techniques are already optimized).

Worksheets

An intermediate process was needed to help produce simple estimates of the X-ray energy flux at a detector for a given geometry. Two spreadsheets were written to satisfy this purpose. The first spreadsheet estimates the total single scatter fluence at the detector. The second spreadsheet predicts the flux vs time for single-scatter x rays. The spreadsheets are named "notime" and "time". Both spreadsheets were prepared using Lotus 1-2-3 version 2.2.

Notime. The first spreadsheet uses a relatively unsophisticated Monte Carlo technique that calculates a contribution from 3000 random x rays. Notime assumes a parabolic scatterer with a point detector located 490 cm from the X-ray source. The spreadsheet accepts three inputs for its calculation, the A and B parameters from equation 1 and a mean free path in cm for the scatterer. A tunnel length of 90 cm is assumed for all calculations and any photons whose path to the detector goes through the tunnel wall are killed. The neutron shield is 1 meter in length and subtends the same solid angle as the tunnel opening.

Since only first scatters are considered, the problem is modelled with only two dimensions (x,y). This is possible because the geometry is symmetric about the x axis. Each particle is born with a random angle of motion θ with respect to the x-axis determined by the equation

$$\theta = \cos^{-1}(1 - 2p_1)$$

where p_1 is a random number between 0 and 1. This accounts for the larger probability of scattering at an angle with a greater $d\Omega/d\Theta$ such as in the vicinity of $\Theta=90°$ where Ω is the solid angle. The first scatter point is determined by this angle and the distance it travels through the scatterer as determined by relating the cumulative probability of having scattered to a random number through the equation

$$\frac{\int_0^d e^{-l/\lambda} dl}{\int_0^\infty e^{-l/\lambda} dl} = p_2'$$

$$p_2' = \lambda(1 - e^{-d/\lambda})$$

$$d = \lambda \mathrm{Ln}(1 - p_2') = \lambda \mathrm{Ln}(p_2)$$

where lambda is the mean free path

After determining the random angle and the random distance travelled in the scatterer, the position of the first scatter is determined by calculating the point where the particles path intersects the parabola and adding the x and y components of d to get x_{fs}, y_{fs}. The first task involves using the quadratic formula to determine the coordinates

where a line with angle Θ and origin 0,0 intersects the parabola. The second task adds d*cos(Θ) and d*sin(Θ) to the x,y intersection points.

Once the position of the first scatter has been determined, a relative contribution is calculated based on the position of the detector. Attenuation factors are calculated for the path length through the scatterer, path length through the neutron shield, and spherical divergence. Other factors used include Klein-Nishina scattering probabilities and Compton energy shifts. (See Appendix B)

Each particle contributes an energy fluence to the detector based on these factors. The numbers calculated have no meaningful units. They are only used for comparison between various parabolas and densities to assist in selecting geometries worthy of further consideration.

Time. "Time" parallels "notime" in most of its calculations. The contribution or weight of a particle is calculated in the same manner for both spreadsheets. "Notime" uses the location of the first scatter to calculate the distance to the first scatter from the source and the distance from first scatter to the detector. Since the particles being modeled are x-rays which travel at a constant speed the arrival time is simply calculated by the equation

$$t_1 = \frac{\sqrt{x_{fs}^2 + y_{fs}^2} + \sqrt{(x_{fs}^2 - 500) + y_{fs}^2}\, cm}{30.0 cm/nS}$$

The particles are sorted by arrival time and totals are calculated for time bins of 0.25-nS width. Obviously, neglecting the contribution of multiple scatters will underestimate the pulse width since particles scattered more than once will have a larger average path length. This spreadsheet was intended to help demonstrate the effects different geometries would have on the pulse shape, not to determine the actual pulse shape.

Both spreadsheets are used only for x rays and neglect any contribution from the outer wall. In fact the paraboloids are assumed to be infinite in size. This approximation is permissible due to the open ended nature of

paraboloids. Any scatters which take place at unreasonable distances will make negligible contributions. The individual particles used are not assigned an energy. The mean free paths, energy shifts, and scatter angle probabilities are normalized for a 10-keV Planckian.

The disadvantage of the time spreadsheet lies in its calculation time. A 5000 particle simulation takes about 15 minutes on a 10-Mhz AT clone with an 80287 math co-processor. Because of RAM limitations, the spreadsheet actually performs calculations for about 200-250 particles. Advanced macros are used to repeat calculations and track totals. "Notime" requires fewer particles because they are not partitioned into time bins and it runs more quickly because it is relieved of sorting the particles by arrival time. Notime can run 3000 particles in about 3 minutes. Clearly the use of first scatters is the principle weakness of the two models. Addition of even a second scatter contribution would quickly complicate the problem beyond reason.

The strength of the spreadsheets lies in their ease of operation. Parameters are simple to enter with little chance of error and the output is easily read. One keystroke produces a plot of the pulse shape vs time.

Both spreadsheets perform calculations that could have been accomplished by writing a small program instead of a spreadsheet. The spreadsheets were used because intermediate results are easily viewed, simplifying debugging and modification. The spreadsheets also simplify the input procedure and can be automated through macros without undue effort. Some sample spreadsheet results can be seen in Appendix C.

III Results and Analysis

Gamma Rays

The NP mode of MCNP was a major disappointment. Using 50,000 source neutrons did not produce enough photons for good statistics. Increasing the number of particle histories was impractical because NP run times were already about 50 minutes (CPU time). PWT cards were added to the input file to split any photons that were created into multiple photons of lesser weight. Relative errors still remained above .5. Fortunately, gamma energy fluxes were averaging about two orders of magnitude less than the neutron fluxes. Because of the high relative errors, the gamma flux figures will not be reported.

Tunnel Length

The tunnel length tests were conducted with a scatterer described by equation 1 inputs of A = 0.02, B = 20. Three different tunnel lengths were evaluated: 90 cm, 140 cm, and 190 cm. The X-ray flux pulse shape and the per particle X-ray/Neutron energy fluences are shown on Figure 3.1 and Table 3.1 respectively. In each case the paraboloid extended parallel to the start of the tunnel.

Not surprisingly, the longer tunnel lengths reduced the X-ray flux. Increasing the tunnel size decreases the por-

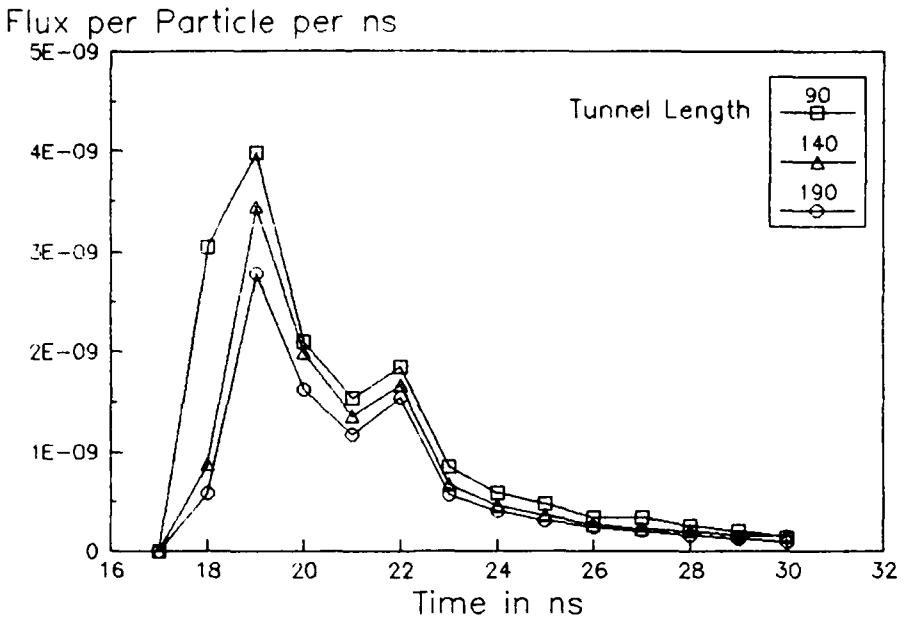

Figure 3.1: Tunnel Effects

tion of the scatterer that has a direct path to the target. By varying the neutron shield angle to exactly match the path to the mouth of the tunnel, the neutron energy fluence was kept virtually constant and in fact decreased for smaller tunnel sizes. This reinforces the utility of the neutron shield and the dominance of forward scattering in neutron collisions. Because it produces the maximum X-ray fluence and the minimum neutron fluence, the 90 cm tunnel was used for all remaining calculations.

Table 3.1: Tunnel Length Energy Fluences

Tunnel Length (cm)	X-Ray Flux (MeV/cm²)	R	Neutron Flux (MeV/cm²)	R	FWHM (ns)
90	1.67E-08	0.04	1.13E-06	0.032	2.54
140	1.44E-08	0.05	1.16E-06	0.042	2.09
190	1.23E-08	0.06	1.21E-06	0.098	2.15

Paraboloids

Six different paraboloid shapes were sampled. B values of 20, 50 and 80 cm were used along with A values of 0.01 and 0.02. The smaller A value represents a thinner parabola with a greater solid angle having a direct path to the target through the tunnel. This shape's advantage is achieved at the expense of pulse shape as the path length difference is small for scatters at different points on the paraboloid's surface. Increasing B shifts the scatterer away from the target, increasing the path length difference while decreasing the total fluence slightly. Figures 3.2 and 3.3 display the pulse shapes and Table 3.2 displays the fluences.

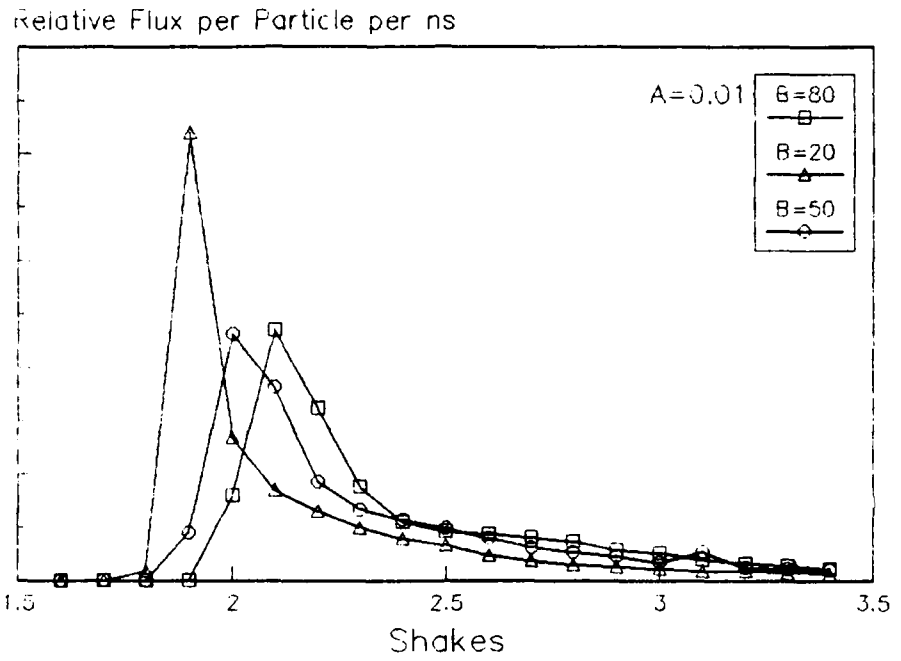

Figure 3.2: Geometries #1

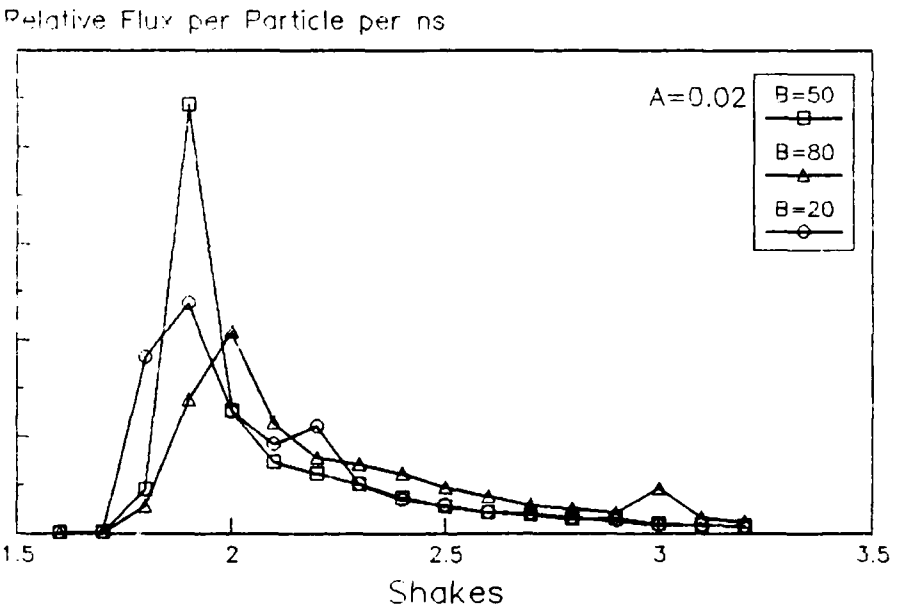

Figure 3.3: Geometries #2

Two runs produced inexplicably high R values for the X-ray fluence estimates. This was not expected since there was little difference between the six geometries. All six shapes provided the same unfavorable characteristic in the FWHM. The target value is not even approached with any shape tested. The FWHM values are estimated from a linear interpolation of the time bin totals. The 1 ns time intervals are far too large to resolve peaks of such small time width. For this reason, the FWHM estimates are very rough approximations at best.

Table 3.2: Paraboloid Energy Fluences

A,B	X-ray	R	Neutron	R	FWHM(nS)
.01,20	2.26E-8	0.205	7.2E-7	0.041	1.25
.01,50	1.65E-8	0.014	na		2.37
.01,80	1.57E-8	0.024	4.3E-7	0.100	2.36
.02,20	1.67E-8	0.045	1.1E-6	0.033	2.55
.02,50	2.07E-8	0.270	9.7E-7	0.067	1.26
.02,80	1.51E-8	0.031	8.7E-7	0.118	2.57

Since the pulse shape information is poor, the fluence totals were used to select an "optimum" shape. Using this criteria the choice here is as expected A=.01 B=20. This shape gave the largest fluence while furnishing the smallest

FWHM. It is a logical choice since the next parameter, density, should provide a marked improvement in pulse shape for a small loss in total fluence.

Density

The benefits of decreasing the scatterer density are clear. The mean free path (MFP) for X-rays is around 7.25 cm in the scatterer (as calculated by MCNP for the 10 keV spectrum). The mean free path is inversely proportional to the material density. The decrease in density will certainly increase the path length to the target based on the corresponding increase in the MFP. Possible adverse side effects include a decrease in fluence due to the tungsten tunnel. The larger MFP will produce more scatters at large angles with respect to the target.

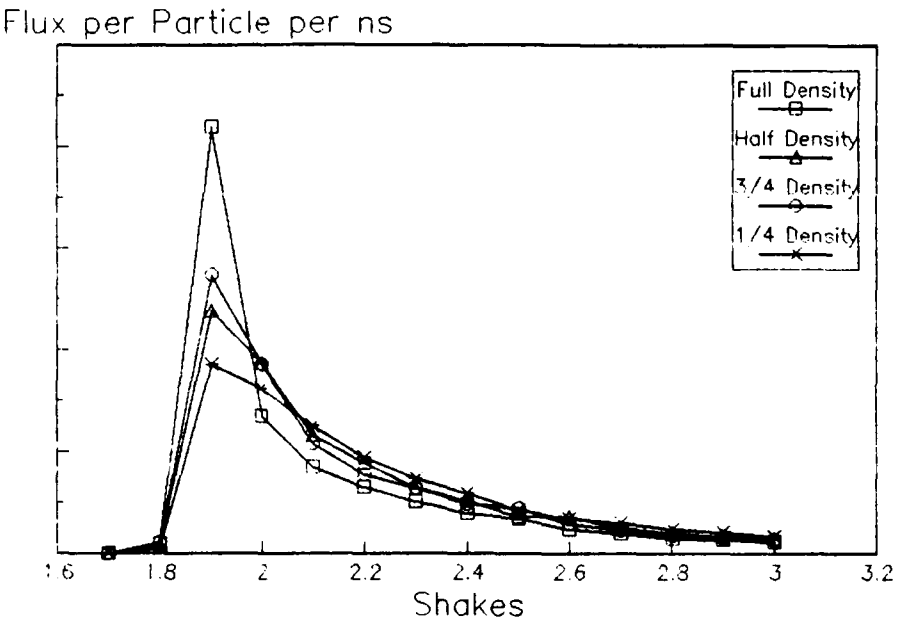

Figure 3.4: Density Effects

Table 3.3: Density Effects

Density	X-ray Fluence (MeV/cm²)	R	Neutron Fluence (MeV/cm²)	R	FWHM (ns)
Full	2.26E-8	0.205	7.17E-7	0.041	1.25
3/4	1.57E-8	0.010	1.09E-6	0.077	2.47
1/2	1.46E-8	0.013	2.46E-6	0.409	2.14
1/4	1.29E-8	0.024	1.09E-6	0.143	3.59

The variation of the density produced the expected results. The pulse width was broadened at little expense to the neutron fluence (note: the neutron input spectrum was switched to the Gaussian fusion spectrum for these and

future calculations). This was by far the most successful attempt at stretching the pulse shape. The variation of scatterer density is limited only by the size limitations of the outer shell and the need to simulate a plane wave.

Uniformity

The uniformity of dose is determined by using multiple type 5 detectors of radii 100, 40, and 1 cm respectively. The tallies estimate the energy flux at each distance. The results of this run are shown in Table 3.4.

Table 3.4: Dose Uniformity

Radius	Fluence MeV/cm^2	Error	Percent Change
100cm	1.49E-8	0.1184	82.6%
40cm	1.75E-8	0.0291	97.4%
1cm	1.80E-8	0.0353	

The goal of 80% uniformity is met with this geometry. The relative error of the estimates are higher at the edge, probably due to the tungsten shield adjacent to the detector. For this reason this tally can be expected to be

the most sensitive to which point on the detector is randomly selected for calculating the contribution (See section II, Variance Reduction).

Dose/Dose Rate

The dose and dose rates were calculated by adding a 20-micron thick disk of silicon at a distance of 489.9 cm from the source. This is the maximum distance a 1 meter radius disk can be from the center of the 5 meter sphere. 500,000 source particles were used for the calculation. The calculation used the type 6 tally which gives the energy deposited in a cell with units of MeV/gram. This value is converted to rads by multiplying it with a conversion factor of 1.602E-8 Rads/(MeV/gram). Figure 3.5 shows the dose per source X-ray deposited in 1 nanosecond intervals (The values could therefore be interpreted as the bin average dose rate in units of rads/ns). A similar calculation was performed for the Pac-Man geometry and the results are shown in the same figure.

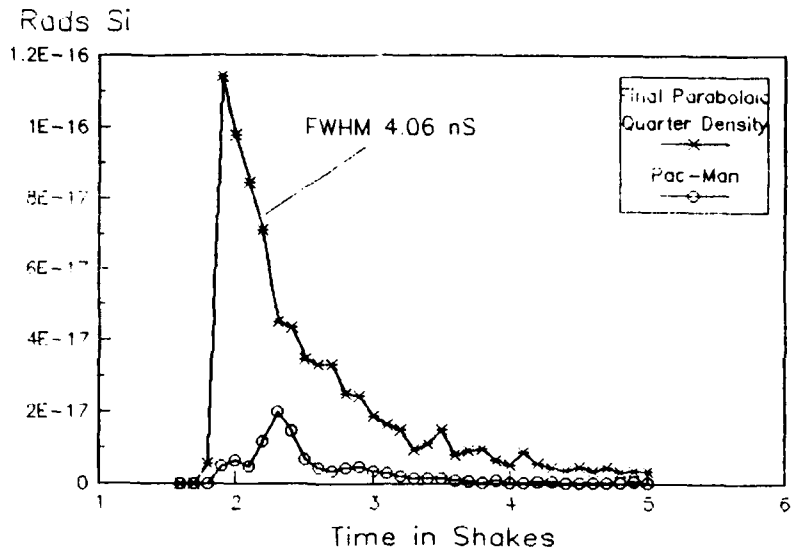

Figure 3.5: X-Ray Doses

Table 3.5: Dose Calculations (Rads(si))

	Paraboloid	R	Pac-Man	R
X-Ray	7.95E-16	0.0164	1.05E-16	0.0251
Neutron	8.56E-17	0.0573	6.38E-17	0.2885
Gamma	4.28E-17	0.099	1.10E-16	0.1959
N/X-ray Ratio	0.19%		1.08%	
G/X-ray Ratio	0.09%		1.87%	

Table 3.5 shows the total doses for both geometries. These tabulated values are also doses per source particle. The ratio of X-ray to neutron dose, or X-ray to gamma dose,

depends on the ratio of source neutrons to source X-rays (note: the gamma tallies are gamma dose per source neutron). This ratio is calculated by the average source particle energy.

The average source particle energy is provided in the MCNP output if the print option is specified in the input file. The neutron and X-ray averages are 14.07 Mev and 31.41 keV respectively. The energy averages also provide the totals 1.99E20 x rays/MJ and 4.44E17 neutrons/MJ which can be used for calculating dose per source energy. Including the 8:1 neutron to photon energy partition the following ratio is calculated.

$$\left(\frac{14{,}070 keV/neutron}{31.414 keV/photon}\right)\left(\frac{8J(neutron)}{1J(photon)}\right) = 56.01\,\frac{Photons}{Neutron}$$

This number was used to calculate the dose ratios in table 3.5.

The paraboloid easily met the 1% ratio requirements and produced a much larger X-ray dose than the current geometry. The Pac-Man calculation produced considerable errors in spite of the 500,000 particles. The gamma dose exceeds the neutron dose on the current geometry perhaps in part due to the absence of the tungsten shield.

IV Conclusions and Recommendations

Summary

Fusion of a DT fuel pellet can provide a X-ray source for preforming X-ray simulation testing. A parabolic scatterer of LiH can be used to temporally spread a delta function X-ray source to control the dose rate on a silicon wafer. The specification for the desired source include specific pulse shape characteristics, fluence uniformity, and maximum neutron and gamma dose contributions.

Calculations were performed on various parabolic geometries to determine the effects of various parameters such as tunnels surrounding the silicon target, paraboloid shape, and scatterer density. The uniformity and neutron/gamma criteria were met but a major problem was encountered in the pulse shapes. Specifications mandate a full width at half maximum on the order of 10s of ns but the best FWHM produced was 4.06 ns.

A tungsten tunnel of 90 cm length was chosen to help shield the target from gammas produced at the outer wall of the fusion chamber. Comparison with the current "Pac-Man" configuration indicate this purpose was achieved as the gamma dose decreased by a factor of 2.

The paraboloid shape chosen is described by the equation

$$x = 0.01\frac{cm}{cm^2}(y^2 + z^2) - 20cm$$

This shape produced the largest X-ray fluence at the target of the six shapes tested.

The most valuable tool for stretching the pulse was variation of the scatterer density. A one quarter density scatterer achieved the best pulse shapes. The utility of decreasing the density of the scatterer is restrained by the finite chamber size and the fact that the effect of the scatterer's shape will become obscured for a sufficiently low density.

The final geometry exceeded the original geometry in all specifications including an increase in total X-ray dose by a factor of 7. Still major improvements will be needed to match the temporal specifications.

Recommendations

MCNP run times must be improved to allow more data collection. One variance reduction technique with great promise is the dxtran process. Dxtran produces psuedo-particles at the surface of a dxtran sphere. Placing the silicon target in the dxtran sphere may allow direct dose calculations within acceptable CPU run times.

More advanced geometries may be needed; there are many possible experiments in this area. Moving the scatterer off axis would destroy the symmetry, perhaps flattening the pulse shape. Using a scatterer of variable density may help spread the pulse shape though this may make manufacturing more difficult and would certainly be difficult to simulate with MCNP. A key to expanding the pulse may be in increasing the number of scatters en route to the target, adding a dense scatterer to areas without a direct path to the target might help increase the path length to the detector. Using two scatterers with a gap between them could possibly produce two different peaks whose sums provide the required pulse shape.

Selecting an optimum geometry is difficult because there are so many different input parameters to the scatterer geometry and there are multiple specification requirements. The task of selecting an optimum requires the establishment of selection criteria for weighting the importance of the various requirements.

Upon selecting a suitable geometry, all calculations should be repeated for a series of monoergic sources for both photons and neutrons. This would allow easy calculation of actual doses for any input spectra by a superposition summation of the individual per source particle responses.

Goals for X-ray to neutron dose ratio and dose uniformity were both met while making significant improvements in the total X-ray dose incident on the target. However, meeting the required dose rate specifications has proven to be an elusive task. Much work is yet to be done if the desired temporal characteristics are to be attained.

Conclusions

Temporal stretching the X-ray pulse must a the primary concern of any future work. The sampling of only six shapes is wholly inadequate for determining an optimum shape. Developing a parametric curve fit by a more systematic variation of the input parameters would be very useful if possible.

Appendix A

Sample Input

Below is a sample input file for MCNP. Brief descriptions and examples follow the listing. More detailed information is available in the MCNP manual.

```
1     1 -0.6 8 -10 -9      $ neutron scatterer parab
2     0 -3  2 -13             $ void outside parab
3     6 -19.3 -3 13 14 -15   $ void outside parab
4     1 -0.6 -2 1 -13      $ LiH scatterer
5     2  -1.0 3 -4        $ hcosi
6     3  -11.36 4 -5      $ Pb
7     4  -0.534 5 -6      $ Li
8     5  -1.0 6 -7         $ Borated Water
9     0 9 -1 -13           $ void
10    0 -8 -1              $ void/source
11    0  8 -9 -1 10 -11   $ void inside parab
12    0  8 -9 -1 10 11    $ void inside parab
13    0  7                $ world
14    0 -3 13 #3          $ void outside parab

1     SQ 0 .01 .01 -.5 0 0 -20 0 0 0
2     SQ 0 .0065 .0065 -.5 0 0 -50 0 0 0
3     SO 500
4     SO 504
5     SO 505
6     SO 506
7     SO 556
8     SO 25
9     SO 125
10    KX 0 .0625 1           $ neutron reflector
11    PZ 0
12    PX 50
13    PX 400
14    CX 100
15    CX 104

MODE   P
SDEF   X 0 Y 0 Z 0 ERG D2
SI2   .01 .02 .03 .045 .07 .1 .15
SP2   .0 .263 .231 .214 .12 .022 .002
M1    3006 .478 3007 .022 1001.04 .5
M2    1001.04 .38 6012 .253 8016 .245 14000 .122
M3    82000 1
```

```
M4     3007 .925 3006 .075
M5     1001.04 .65 8016 .334 7014 .003 5000 .013
M6     74000.35 1
*FX5:P 489.89 100 1
E5     .010 .030 .050 .080 .110 .150
T5     1.6 1.7 1.8 1.9 2.0 2.2 2.4 2.6 2.8
       3 3.2 3.4 3.6 3.8 4 4.2 4 4.6 4.8 5 6
IMP:P 40 40 40 40 8 4 2 1 40 40 40 40 0 40
CUT:P   6 0
NPS    50000
```

The first section of the input file is the cell definition section. Each line defines a cell in terms of its material, the material density, and the surfaces which bound it. For example cell 1 contains material 1 with a density of 0.6 g/cm^3 and is bound by surfaces 8, 9, and 10.

The second section describes the surfaces. The first two letters designate the surface type such as CX for a cylinder parallel to the X-axis, PX for a plane perpendicular to the X-axis, etc.. For example, surface three is a sphere with its center at the origin and a radius of 500 cm.

The third section defines the problem by specifying the rest of the necessary inputs. This problem is a photon transport problem as specified by the MODE P entry. The source is defined by the SDEF, SI, and SP entries as a histogram distribution. The material cards specify the elements presently in terms of their atomic number and atomic mass and can optionally specify a cross section table. Each element in the material has a relative abundance specified as well. The tally type selected is *F5 for ring detector with

units MeV/cm^2. The T5 and E5 entries tell MCNP to partition the tally into time and energy bins. The IMP card specifies the relative importance of the different cells, and is used for splitting and Russian roulette. CUT tells MCNP what the cut-off levels are for energy, time and weight and NPS is the number of particles to be run. Clearly-defined sample inputs are available in the MCNP manual.

The material densities used in all calculations are shown in table A.1.

Table A.1: Material Densities

Material	Density (g/cm^3)
LiH	0.6 (3:22)
Silicon	2.33 (10:496-8)
Tungsten	19.3
Hydrocarbon	1
Lead	11.36
Lithium	0.534
Borated Water	1

The paraboloids are actually the volume between two paraboloids. There were seven different paraboloid pairs used in this report. Each paraboloid is describe by the parameters of equation 1 as shown in table A.2. LiH was

treated as a cheap resource in this report. The parabolic scatterers are considerably larger than the pac-man scatterer with masses in the range of 3-4 metric tons. Large mass reductions could certainly be accomplished with only small losses in total fluence at the target.

Table A.1: Paraboloid Geometries

Inside Paraboloid		Outside Paraboloid	
A	B	A	B
0.02	20	0.015	40
0.02	50	0.015	70
0.02	80	0.015	100
0.01	20	0.0065	50
0.01	50	0.0065	80
0.01	80	0.0065	110
0.01	20	0.008	45
0.01	20	0.007	50
0.01	20	0.0045	70

Appendix B

Klein-Nishina Table

The Klein-Nishina formula describes the anisotropic nature of Compton scattering. The relative probability of scattering at an angle theta is a function of both theta and the photon energy as described by the relationship

$$\frac{d\theta}{d\Omega} = k(1+\alpha(1-\cos(\theta))^{-3}(1+\cos^2(\theta)))(1+\frac{\alpha^2(1-\cos(\theta))^2}{[1+\cos^2(\theta)](1+\alpha[1-\cos(\theta)])})$$

where alpha is the ratio of the photon energy to the electron rest mass energy. The energy dependence of this equation can be seen in figure B.1. (11:65-68)

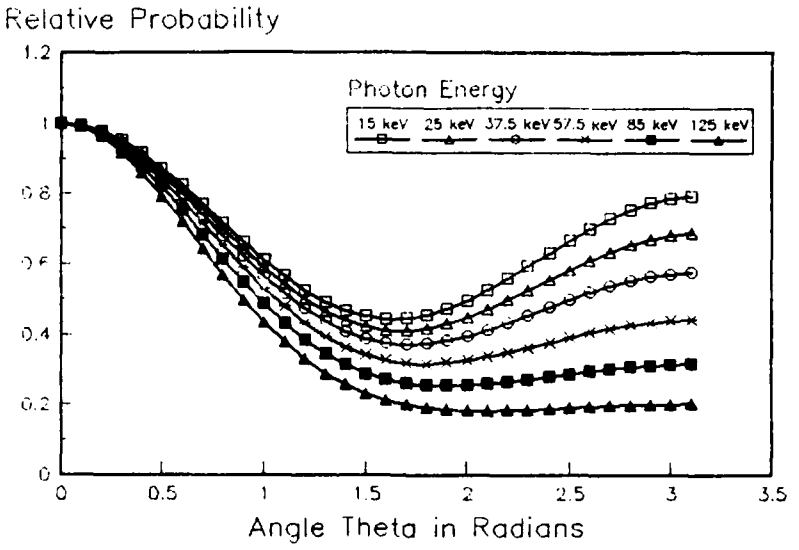

Figure B.1: Klein-Nishina Distribution

The relative probability per unit solid angle of scattering at angle theta was calculated for over one hundred angles between 0 and π for each of six energies. These probabilities were weighted based on the magnitude of a 10-keV Planckian distribution at that energy and the weighted sum of these calculations provided a table of weighting factors which was crudely normalized for a 10-keV blackbody distribution. Since the energy flux, not the number flux, is more important for this exercise, another factor was incorporated. Photons undergo an energy shift after Compton scatters. This shift is described in the following equation.

$$\frac{E'(\theta, E)}{E} = \frac{1}{1 + \frac{E}{511 keV}(1 - \cos\theta)}$$

This factor was added to represent the energy incident on the point detector. The energy shift information had to be added before summing the individual energy tables because of the energy dependence of the equation.

The spreadsheets "time" and "notime" calculate the angle from the first scatter to the detector. This angle is used to look up the weighting factor by finding the largest angle in the table not larger than the calculated angle. No interpolation is used because of the high angle density of the table (0.01 radians). The approximations and round off errors inherent in this method should be small in comparison to the effect of using only single scatters in the model.

Appendix C

Spreadsheet Samples

Sample outputs from the time and notime spreadsheets are presented without discussion below. Table C.1. shows the relative energy fluence for three parabolas. No units are implied for the fluence. Note sigma is a sample standard deviation, not a relative error. Sample single-scatter flux distributions are shown in figures C.1 and C.2 for different shapes and scatterer densities. Recall the tungsten tunnel does not appear in either spreadsheet model.

Most of the data obtained from the spreadsheet was discard since it was intended as an intermediate approximation. The importance of multiple scatters in the actual energy fluence limit the utility of the spreadsheet results. The nature of spreadsheet models precludes presenting the source "code" here.

Table C.1: "Notime" Sample Results

B=20 cm

A(1/cm)	0.05	0.02	0.01
Relative Fluence	0.095	0.165	0.17
σ	0.023	0.024	0.018

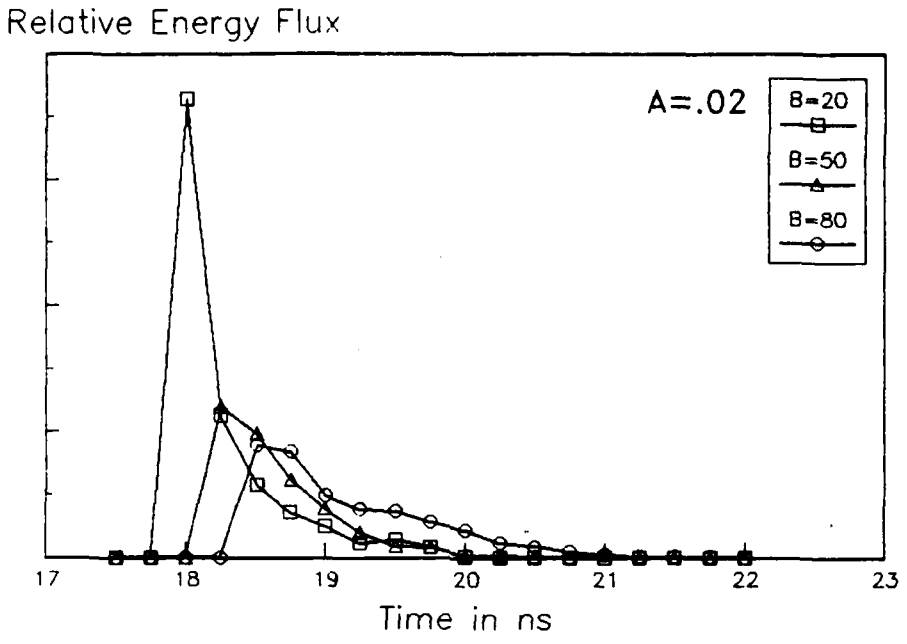

Figure C.1: Spreadsheet Flux Estimate #1

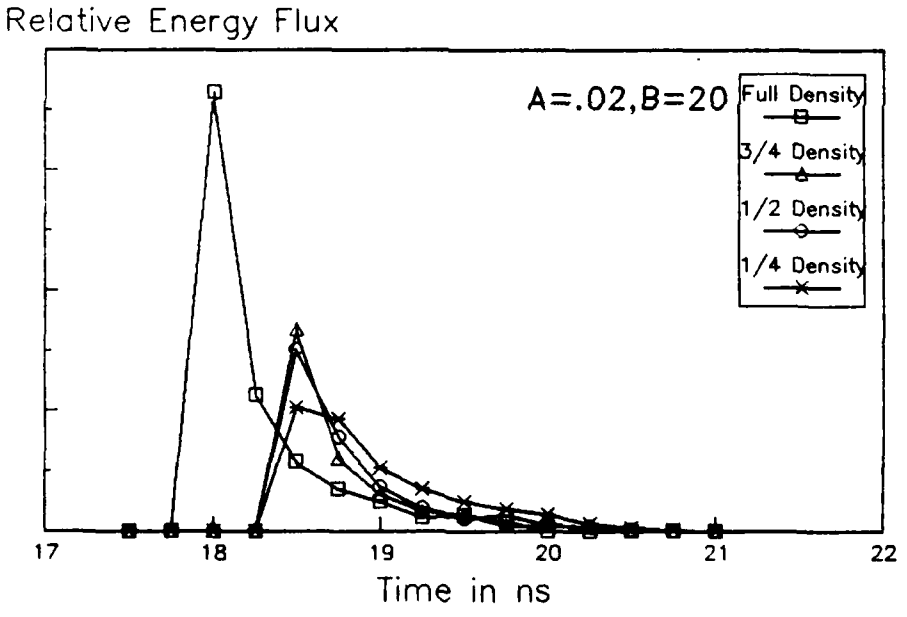

Figure C.2: Spreadsheet Flux Estimate #2

References

1. Johnson, Thomas H. "Inertial Confinement Fusion: Review and Perspective", Proceedings of the IEEE, Vol 72, Number 5, 548-594, May 1984.

2. Dolan, Thomas James. Fusion Research, Vol II, Experiments, Pergamon Press, New York, 1982.

3. Nichols, Lieutenant Don F. Spectral and Temporal Fidelity of a Hard X-Ray Effects Simulation Test in a High Gain ICF Facility. MS thesis, AFIT/GNE/ENP/89M-6, School of Engineering, Air Force Institute of Technology (AU), WPAFB OH, March 1989

4. Messenger, G. C. and M. S. Ash. The Effects of Radiation on Electronic Systems, Van Nostrand Reinhold Co., New York, 1986.

5. Beller, Major Denis E. Professor of Nuclear Engineering, Personal Communication, AFIT, WPAFB OH, 19 December 1989.

6. Tobin, Michael T., ICF Group,Personal Comunication, Lawrence Livermore National Laboratory, Livermore CA, 22 August 1989.

7. Glasstone, Samuel and Phillip J. Dolan. The Effects of Nuclear Weapons (Third Edition), U.S. Department of Defense, Washington D.C., 1977.

8. Los Alamos National Laboratory, MCNP-A General Monte Carlo Code for Neutron and Photon Transport, LA-7396-M, Rev. 2, September 1986

9. Little, Robert C. and Robert E. Seamon, "Nuclear Data for MCNP", Monte Carlo Methods and Applications in Neutronics, Photonics and Statistical Physics, Proceedings of the Joint Los Alamos National Laboratory, 13-25, 22-26 April 1985.

10. Wehr, M. Russell et al. Physics of the Atom (Third Edition), Addison-Wesley Publishing Company, Reading Massachusetts, 1978.

11. Knoll, Glenn F. Radiation Detection and Measurement, John Wiley and Sons, New York, 1979.

REPORT DOCUMENTATION PAGE

Form Approved
OMB No. 0704-0188

1a. REPORT SECURITY CLASSIFICATION UNCLASSIFIED	1b. RESTRICTIVE MARKINGS
2a. SECURITY CLASSIFICATION AUTHORITY	3. DISTRIBUTION/AVAILABILITY OF REPORT Approved for public release; distribution unlimited
2b. DECLASSIFICATION/DOWNGRADING SCHEDULE	
4. PERFORMING ORGANIZATION REPORT NUMBER(S) AFIT/GNE/ENP/90M-7	5. MONITORING ORGANIZATION REPORT NUMBER(S)
6a. NAME OF PERFORMING ORGANIZATION School of Engineering 6b. OFFICE SYMBOL (If applicable) AFIT/ENP	7a. NAME OF MONITORING ORGANIZATION
6c. ADDRESS (City, State, and ZIP Code) Air Force Institute Of Technology (AU) Wright-Patterson AFB, OH 45433-6583	7b. ADDRESS (City, State, and ZIP Code)
8a. NAME OF FUNDING/SPONSORING ORGANIZATION 8b. OFFICE SYMBOL (If applicable)	9. PROCUREMENT INSTRUMENT IDENTIFICATION NUMBER
8c. ADDRESS (City, State, and ZIP Code)	10. SOURCE OF FUNDING NUMBERS PROGRAM ELEMENT NO. / PROJECT NO. / TASK NO. / WORK UNIT ACCESSION NO.
11. TITLE (Include Security Classification) see block 19	
12. PERSONAL AUTHOR(S) Russel L. Tinsley, B.S., CAPT, USAF	
13a. TYPE OF REPORT Thesis 13b. TIME COVERED FROM _____ TO _____	14. DATE OF REPORT (Year, Month, Day) 15. PAGE COUNT
16. SUPPLEMENTARY NOTATION	

17. COSATI CODES			18. SUBJECT TERMS (Continue on reverse if necessary and identify by block number)
FIELD	GROUP	SUB-GROUP	
19	11		Hard X Rays, Weapons Effects, Inertial Confinement Fusion, LMF, Laboratory Microfusion Facility

19. ABSTRACT (Continue on reverse if necessary and identify by block number)

Title: OPTIMIZATION OF A COMPTON SCATTERER FOR HARD X-RAY EFFECTS SIMULATION IN AN ICF FACILITY

Chairman: Denis E. Beller, Major, USAF
Assistant Proffessor of Engineering Physics

(Abstract on reverse)

20. DISTRIBUTION/AVAILABILITY OF ABSTRACT ☒ UNCLASSIFIED/UNLIMITED ☐ SAME AS RPT. ☐ DTIC USERS	21. ABSTRACT SECURITY CLASSIFICATION UNCLASSIFIED
22a. NAME OF RESPONSIBLE INDIVIDUAL Denis E. Beller, Major, USAF	22b. TELEPHONE (Include Area Code) (513) 255-4498 22c. OFFICE SYMBOL AFIT/ENP

ABSTRACT (continued from block 19)

The MCNP Monte Carlo code was used to examine the optimization of a compton scattere for use in the proposed Laboratory Microfusion Facility.
The LMF will be an inertial confinement fusion facility for the testing of high-gain deuterium-tritium pellets (DT), and will produce a pulse of hard X rays and neutrons over a very short time interval. The original scattere design was a sphericals shell of ^{6}LiH with an inner radius of 1 meter and a thickness of 17.5 cm. Parabolic scatterers were preferable to the original geometry. The optimum parabola produce an x-ray dose of7.95 e-16 Rads (Si) per source X ray vs 1.05 e-16 Rads for the spherical scatterer. Neutron and Gamma doses were held to less than 1% of the x-ray dose. By reducing the scatterer's density to one quarter nominal density the x-ray pulse was widened to a full width at half maximum (FWHM) of 4.06 ns.
All characteristics of the x-ray pulse were improved by the use of a parabolic compyon scatterer.